Characterisation of the electromagnetic component in ultra-high energy inclined air showers

I. Valiño[a,*], J. Alvarez-Muñiz[b], M. Roth[a], R.A. Vazquez[b], E. Zas[b]

[a] *Karlsruhe Institute of Technology, POB 3640, D-76021 Karlsruhe, Germany*
[b] *Instituto Galego de Física de Altas Enerxías and Departamento de Física de Partículas, Universidade de Santiago de Compostela, Spain*

Abstract

Inclined air showers – those arriving at ground with zenith angle with respect to the vertical $\theta > 60^\circ$ – are characterised by the dominance of the muonic component at ground which is accompanied by an electromagnetic "halo" produced mainly by muon decay and muon interactions. By means of Monte Carlo simulations we give a full characterisation of the particle densities at ground in ultra-high energy inclined showers as a function of primary energy and mass composition, as well as for different hadronic models assumed in the simulations. We also investigate the effect of intrinsic shower-to-shower fluctuations in the particle densities.

Key words: Cosmic rays, Extensive air showers, Ground detector, Simulation, Muon component, Electromagnetic component
PACS: 96.50.S, 96.50.sd, 13.85.Tp

1. Introduction

Inclined air showers are conventionally defined as those arriving at ground with zenith angles θ above 60°. At large zenith angles the electromagnetic (EM) component in air showers, mainly produced by the decay of π^0s, is largely absorbed in the greatly enhanced atmospheric depth the shower needs to cross before reaching ground, so that in a first approximation only the more penetrating particles such as muons survive to ground. Muons are accompanied by an electromagnetic component produced mainly by muon decay in flight and muon interactions such as bremsstrahlung, pair production and nuclear interactions. A full characterisation of this so-called electromagnetic "halo" is given in this work.

The study of inclined showers is of great interest because their detection immediately enhances the exposure of existing air shower detectors by up to about

*Corresponding author. Present address: Institut für Kernphysik, Karlsruhe Institute of Technology, D-76021 Karlsruhe, Germany. Tel: +49 (0) 724782-4978.
Email address: inesvr@gmail.com (I. Valiño)

30% with respect to that achieved with vertical showers ($\theta < 60^\circ$), extending the field of view to sky directions otherwise inaccessible.

Inclined showers have been detected in the past in arrays of ground detectors such as the Haverah Park [1] and AGASA [2] experiments. Modern detectors such as the Pierre Auger Observatory [3] or the Telescope Array [4, 5] can also be used to detect showers with large zenith angles. In particular, the Surface Detector Array (SD) of the Pierre Auger Observatory is well suited to detect very inclined showers at energies above about 5×10^{18} eV, with high efficiency and unprecedented statistical accuracy. The energy spectrum of Ultra-High Energy Cosmic Rays (UHECR) with inclined showers was recently measured [6]. The surface detector is an extended array of deep water Cherenkov detectors that act like volume detectors adequate for recording particles arriving at ground at all zenith angles.

As in all ground arrays, the distribution of the detector signals produced by shower particles is used to estimate shower observables such as the primary energy and to perform composition studies. As shown in previous works [7, 8], the specific characteristics of inclined showers entail that their analysis requires a different approach from the standard one for vertical showers. The study of the particle densities of the electromagnetic and muonic components at ground level becomes essential in the reconstruction [9] and analysis of events at large zenith angles.

Inclined showers have also been studied for years for other reasons. In the 70's, it was suggested that showers induced by neutrinos could be identified in the background of inclined proton or nuclei induced showers by searching for deeply penetrating inclined showers [10] which should exhibit a significant electromagnetic component at ground. In this respect the study and characterisation of the electromagnetic halo in inclined showers is also of great importance.

In this paper we have used Monte Carlo generators simulating the air shower development to obtain the particle densities induced by the electromagnetic and muonic components of inclined air showers. In contrast to other works [1, 11] we have performed a comprehensive characterisation of the ratio of the electromagnetic to muonic densities as a function of distance to the shower core for different zenith angles. We have studied the dependences of this ratio on the primary energy, mass composition and hadronic interaction model assumed in the simulations. We have also studied the effect of the geomagnetic field that deviates charged particles along their paths to the detector. As a result of this study we give parameterisations of the average ratio of the EM and muonic components as a function of the distance to the shower core, shower zenith angle (θ) and azimuth angle (ζ) of the position at which the particle arrives at ground with respect to the incoming shower direction, as well as on the distance to the shower core in the shower plane [1].

The effect of the intrinsic shower-to-shower fluctuations on the electromagnetic and muonic contributions to the density has also been studied. Our re-

[1] The shower plane is the plane transverse to the shower axis.

sults are relevant for the reconstruction of inclined showers in ultra-high energy cosmic ray detectors such as the Pierre Auger Observatory and the Telescope Array.

2. Simulation method

2.1. Extensive air shower simulations

We have generated a library of inclined air showers induced by proton and iron primaries using the Monte Carlo shower propagation code AIRES 2.6.0 [12] and the hadronic interaction models QGSJET01 [13] and Sibyll 2.1 [14]. Showers were generated with energies of 1, 10 and 100 EeV, with zenith angle ranging from 60° to 88° in steps of 2° and random azimuth angle (unless otherwise indicated). We have simulated 100 showers for each combination of energy and zenith angle. Showers were simulated with and without geomagnetic field assuming the location of the surface detector of the Pierre Auger Observatory [3] (ground level placed at a depth of 876 g cm^{-2}) and using a curved atmosphere based on the Linsley's atmospheric model [15].

The number of particles that are produced in an air shower at EeV energies and above and the computing time needed to follow all the secondaries is typically excessively large. To avoid this problem, current air shower simulation codes use a statistical sampling algorithm (thinning algorithm) which allows to propagate only a small representative fraction of the total number of particles [16]. Statistical weights are assigned to the sampled particles in order to compensate for the rejected ones. Therefore, the output of the air shower simulation is a detailed data file with weighted entries containing the particle information at ground level. In this work, showers were simulated with a relative thinning level of 10^{-6} and a weight factor for the electromagnetic (heavy) particles of 12 (0.14). Since the thinning process itself introduces artificial fluctuations, for the study of the intrinsic shower-to-shower fluctuations we have also simulated sets showers with a thinning level of 10^{-7}. All the particles with kinetic energies above the following thresholds were tracked: 80 keV for electrons, positrons and gammas, 10 MeV for muons, 60 MeV for mesons and 120 MeV for nucleons and nuclei.

Since the ground arrays differ in detection thresholds and detector response, we have performed particle energy cuts at ground level corresponding to the particular case of water Cherenkov detector thresholds: 264 KeV for electrons and positrons, 1.286 MeV for gammas and 54.6 MeV for muons. Note that the kinetic energy thresholds used in the AIRES simulations for electromagnetic particles are all below the Cherenkov thresholds, implying that we are not artificially eliminating electrons, positrons or photons that could contribute to the electromagnetic densities. Concerning muons, one can see by extrapolating the energy spectrum of muons shown in Fig. 1 that the number of muons below 10 MeV in inclined showers – not accounted for in our AIRES simulations but still being able to produce electrons above the Cherenkov threshold in water – represents a small fraction of the total number of muons.

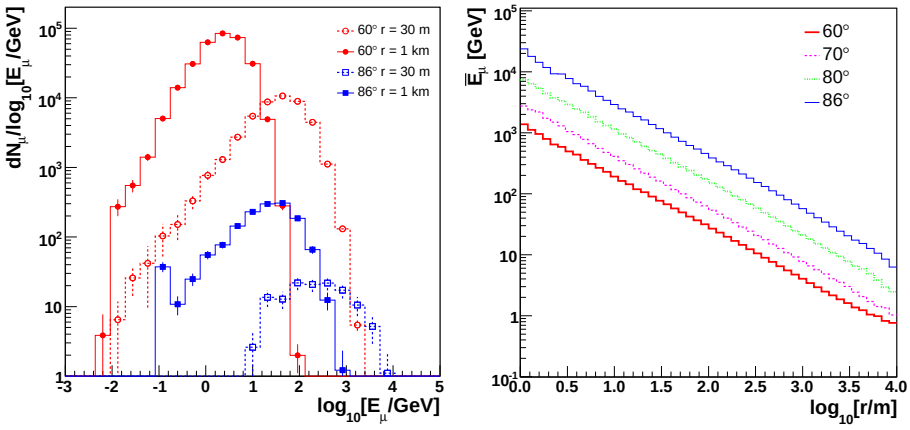

Figure 1: Left panel: Energy spectrum of muons at 30 m (open symbols) and 1000 m (full symbols) to the shower axis in the shower plane for showers at zenith angles 60° and 86°. Right panel: Mean muon kinetic energy as a function of the distance to the shower axis in the shower plane for different zenith angles. The simulations were performed for 10 EeV proton showers with QGSJET01 hadronic model.

2.1.1. Resampling procedure

To calculate the particle densities induced by the electromagnetic and muonic components of the shower, we perform a simple resampling procedure (also called *unthinning* procedure). The particle density is calculated as the sum of the statistical weights assigned by the thinning algorithm of the particles falling in a sampling region divided by its area. The sampling area must be large enough so that a significant fraction of particles falls inside it, but at the same time it should be small enough so that particle properties are representative of their expected properties in the particular region of interest [17]. In this work, we have chosen two different sampling regions in the plane perpendicular to the incoming shower direction (shower plane). On the one hand following the previous criterion,, we have considered particles falling in concentric rings with width of 0.08 in $log_{10}r$ in the shower plane to obtain the particle densities as a function of the distance to the shower axis (lateral density). On the other hand, we have considered square cells of 60×60 m^2 in the shower plane when calculating the two dimensional distributions of the particle densities.

3. The electromagnetic and muonic components in inclined showers

The conventional separation between vertical and inclined showers is based on the zenith angle θ of the arrival direction of the cosmic ray particle that induces the shower. This separation stems from the different atmospheric grammage that the showers have to cross before reaching the ground, which increases approximately as $\sec\theta$. This fact implies that the showers arrive at ground at different stages in their evolution depending on θ.

A hadronic cosmic ray typically initiates an air shower at the top of the atmosphere in the first few 100 g cm^{-2}. The EM component of the shower rises as the shower develops and reaches a maximum at a depth of $X_{\rm max} \sim 800\,{\rm g\,cm^{-2}}$ for a 10 EeV proton shower, close to the total vertical depth of atmosphere for the altitude of the Pierre Auger Observatory. After $X_{\rm max}$, the EM component is rapidly absorbed in the atmosphere mainly due to low-energy ionization processes and the photoelectric effect. Meanwhile, non-decaying muons propagate almost unattenuated to the ground, except for ionization energy losses and deflections in the geomagnetic field. Consequently, a shower arriving with $\theta = 0^\circ$ reaches the ground shortly after shower maximum and the electromagnetic component dominates at ground. However, for showers arriving with $\theta > 60^\circ$ the atmospheric slant depth increases from $\sim 1760\,{\rm g\,cm^{-2}}$ to up to more than 30000 g cm^{-2} for completely horizontal showers. This results in the dominance of the muonic component at ground [18] accompanied by a small electromagnetic component consisting mainly of the remnant of the electromagnetic shower due to cascading processes from π^0 decay of hadronic origin, and the electromagnetic halo due to muon decay in flight and hard muon interactions.

Low energy muons (below a few GeV) typically decay along their paths to the ground generating small electromagnetic subshowers contributing to the particle densities at ground. This component mimics the muon spatial distribution and is proportional to the muon density [19].

Hard muon interactions (pair production, bremsstrahlung and hadronic interactions) become more and more relevant as muon energy increases. To illustrate when these processes are expected to contribute larger to the EM halo, in the left panel of Fig. 1 we show the energy spectrum of muons at distances of 30 m and 1000 m to the shower axis for 10 EeV proton-induced showers at different zenith angles. As shown here, these processes are expected to contribute to the EM halo especially in highly inclined showers in which most of the muons are typically very energetic (hundreds of GeV), because the lower energetic muons typically decay before traveling the enlarged distances from their production height to the ground. Hard muon interactions are also expected to be more frequent close to the shower core where a larger content of energetic muons is expected since energetic muons deviate less from the shower axis.

3.1. Asymmetry of the electromagnetic and muonic densities at ground level in inclined showers

A vertical shower typically exhibits a symmetric pattern of particle densities around the shower core in the shower plane. In the case of inclined showers there are several effects that produce an asymmetry on the pattern of particle densities. The most important sources of which are described below.

3.1.1. Asymmetries due to the geomagnetic field

Muons in inclined showers travel along sufficiently long paths in the atmosphere to be affected by the Earth's magnetic field. Positive and negative muons

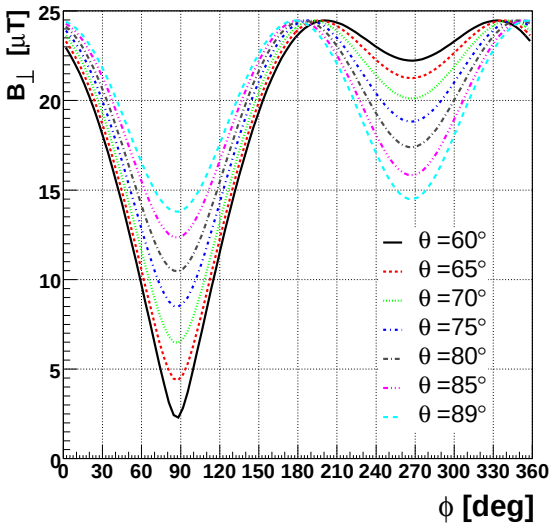

Figure 2: The component of the geomagnetic field perpendicular to the shower axis as a function of the shower azimuth angle for showers arriving with different zenith angles at the location of the Pierre Auger Observatory [2]. $\phi = 0°$ corresponds to the geographical East, and $\phi = 90°$ to the geographical North.

are deviated in opposite directions with respect to the rectilinear trajectories they would follow in the absence of geomagnetic field. As a consequence the field distorts the patterns of the muonic densities in the shower plane producing elliptical or even 2-lobed patterns in very inclined showers at ground, an effect extensively studied in [8, 20]. The degree of distortion and the shape of the pattern depend on the strength and orientation of the magnetic field with respect to the shower axis, namely on the component of the field perpendicular to the shower axis $B_\perp$, as well as on the distance traveled by the muons. This introduces a dependence of the asymmetry on the shower zenith (θ) and azimuth (ϕ) angles. As it was shown in [8] the effect on the muonic distributions is only significant for $\theta \geq 75°$. In Fig. 2 we show $B_\perp$ as a function of ϕ for the particular location of the Southern Pierre Auger Observatory site. For a given zenith angle, the distortion is expected to be maximal close to $\phi = 0°$ and $\phi = 180°$ and minimal around $\phi = 90°$. $\phi = 0°$ points eastwards and is oriented counterclockwise.

As an example of the effect of the geomagnetic field on the particle densities, in Fig. 3 we show 2-dimensional maps of the muonic and electromagnetic particle densities in the shower plane in a 10 EeV proton induced shower arriving at

[2]The geomagnetic field used in this work corresponds to the data of May 2006 extracted from the IGRF database [21] included in AIRES. The strength of the field is 24.472 μT, the inclination angle below the horizon is 35.29° and the declination angle with respect to the geographical North is 2.91°.

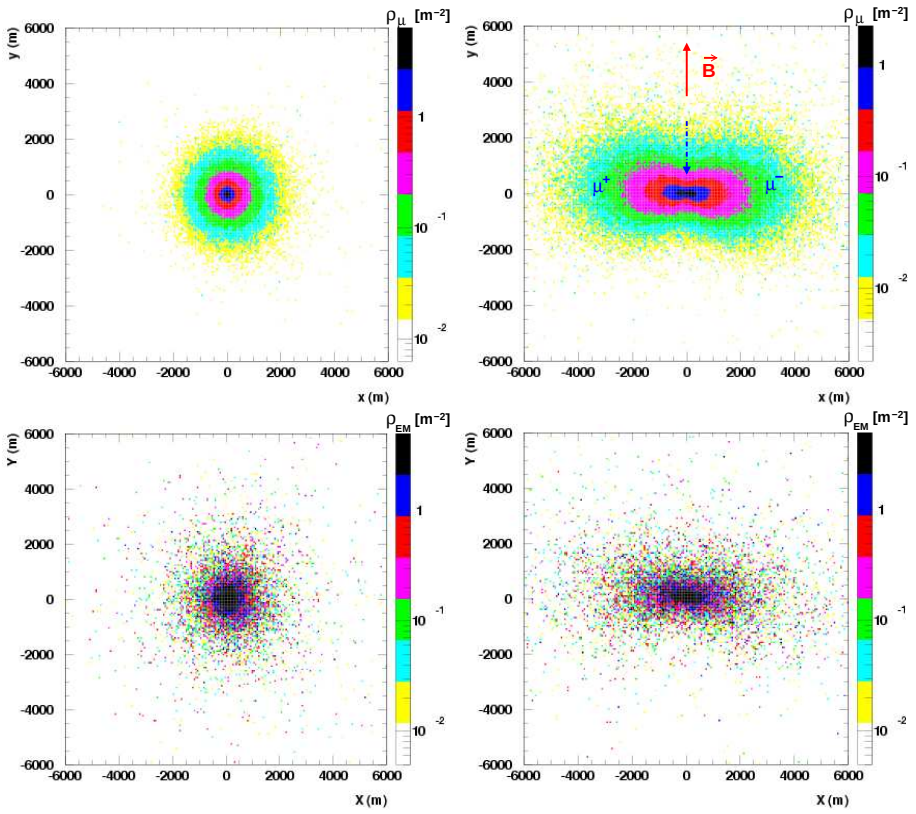

Figure 3: Maps of the muonic (top panels) and electromagnetic (bottom panels) densities in the shower plane in a 10 EeV proton induced shower with a $\theta = 86°$ and $\phi = 90°$. Left panels: Densities without the effect of the geomagnetic field. Right panels: Maps with geomagnetic effect at the location of the Pierre Auger Observatory. The dashed arrow indicates the shower direction projected on the ground. The solid arrow indicates the direction of the total magnetic field $\vec{B}$ after projecting it on the ground. There is a component of $\vec{B}$ perpendicular to the shower axis. The simulations were performed for 10 EeV proton showers with the QGSJET01 hadronic model.

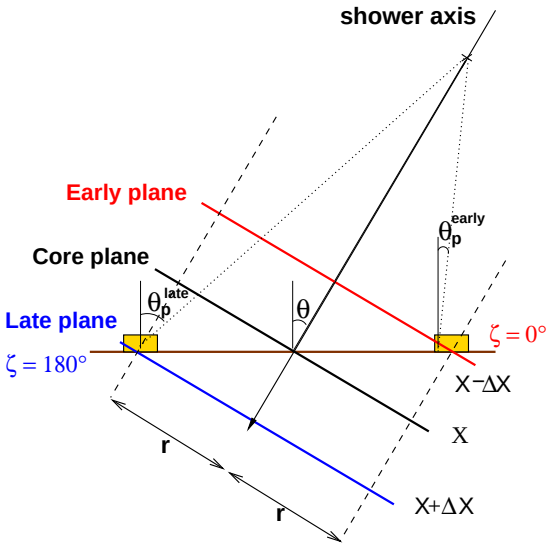

Figure 4: Schematic view of an inclined shower reaching the ground. Three planes are displayed intersecting the ground plane, each one at different depth along the shower development: the early plane, the late plane and the shower core plane. The latter is also called shower plane.

$\theta = 86°$ and $\phi = 90°$, with (right) and without (left) the geomagnetic field induced. The distortion of the cylindrical symmetry of the muonic component is apparent, and since the electromagnetic halo preserves the spatial distribution of muons in inclined showers, the pattern of the electromagnetic particle density exhibits a shape similar to the muonic one, although slightly blurred due to multiple Coulomb scatterings suffered by the electrons before reaching ground.

3.1.2. Asymmetries due to geometrical and shower evolution effects

Besides the asymmetries induced by the geomagnetic field, there is also an azimuthal asymmetry in the muonic and electromagnetic particle densities due to the combination of geometrical and shower evolution effects [22]. As illustrated in Fig. 4 shower particles do not travel parallel to the shower axis in general and therefore they cross different amounts of atmospheric depth before reaching ground. The crossed depth depends on the azimuthal angle (ζ) of the position on the ground at which the particle arrives with respect to the incoming shower direction. In particular, particles arrive at the ground in the *early* region of the shower (the portion of the shower front that hits the ground first corresponding to $\zeta = 0°$) more vertically than those in the *late* region (corresponding to $\zeta = 180°$). This is essentially the basis for the geometrical effect, which depends strongly on the specific characteristics of the detectors sampling the shower front. The asymmetry induced by the geometrical effect is typically small in showers with high zenith angles. The more inclined a shower, the more

energetic the muons arriving at ground are and hence the smaller the difference in the arrival angle distributions between the early and late regions of the shower.

The asymmetry induced by the shower evolution can be understood as follows. Particles at the same distance to the shower axis in the shower plane, but arriving with different azimuthal angles ζ travel along different paths, and belong to different stages in the evolution of the shower. The importance of this effect depends on the evolution of the lateral particle distribution and on the attenuation of the total number of particles with the atmospheric depth. In Fig. 4 the detector in the early region of the shower is hit by a younger stage in the evolution of the shower than the detector in the late region. More quantitatively, for instance in a 10 EeV proton shower at $\theta = 60^\circ$, there is a difference of $2\,\Delta X \sim 370$ g cm^{-2} (for notation see Fig. 4) between the atmosphere crossed by particles produced at the same height, traveling in straight line and hitting the ground in the late and early regions at a distance $r = 1000$ m to the core in the shower plane. This difference increases with the distance from the shower core.

The asymmetry induced by the evolution of the shower affects more the electromagnetic component produced by π^0 decay than the muonic component or its associated electromagnetic halo. The reason is that this component is exponentially suppressed after the shower maximum, and small variations of the depth crossed by the shower induce large differences in the number of electromagnetic particles on the ground. However, the muonic component is less attenuated and therefore the asymmetry induced by this effect is smaller. As a consequence, shower evolution is expected to induce a much smaller asymmetry in the density in showers with zenith angles $\theta > 70^\circ$, because the electromagnetic component from π^0 decay is practically suppressed, and the electromagnetic halo is simply following the pattern of the muonic component where the asymmetry is small. This is shown in Fig. 5 where we plot the relative difference between the electromagnetic and muonic particle densities in the early ($\zeta \approx 0^\circ \pm 15^\circ$) and late ($\zeta = 180^\circ \pm 15^\circ$) regions in the shower plane as obtained in our simulations. For the moment the geomagnetic field effect is neglected in this study. In the left panel of Fig. 5 it can be seen that for showers at $\theta = 60^\circ$ the difference in the electromagnetic density between the early and the late regions is very large even at small distances to the core (for example a factor 1.2 at $r \sim 100$ m), because the electromagnetic component from π^0 decay is still significant in the early region, and it is significantly absorbed before reaching ground in the late region. This difference increases steeply with distance r. However, at $\theta = 70^\circ$ the difference between the densities in the early and late regions is smaller, because the electromagnetic component from π^0 decay is absorbed at all ζ and only the electromagnetic halo remains, except for at very far distances from the core where, besides inheriting the already quite large asymmetry due to the muonic component, there is still some remnant of the electromagnetic shower present in the early region but not in the late one. This explains why the early-late asymmetry follows essentially the behaviour of the corresponding muonic density (right panel of Fig. 5). In the muonic case, the relative difference

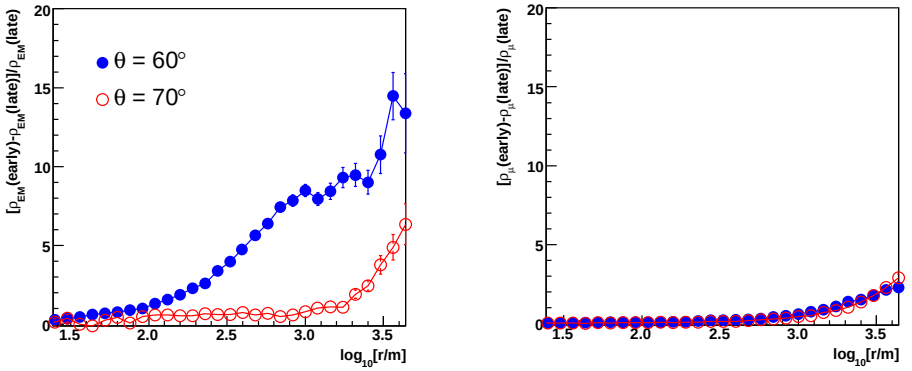

Figure 5: Left panel: Early-late asymmetry of the electromagnetic particle density as a function of the distance from the core in the shower plane for showers at $\theta = 60°$ (full circles) and $\theta = 70°$ (empty circles). Right panel: Early-late asymmetry of the muon particle density as a function of the distance from the core in the shower plane for showers at $\theta = 60°$ (full circles) and $\theta = 70°$ (empty circles). The simulation was performed for 10 EeV proton showers with the QGSJET01 hadronic model.

between the early and late densities is always small regardless of zenith angle.

3.2. The lateral distribution of the electromagnetic and muonic components in inclined showers

The electromagnetic and muonic particle densities have a characteristic behaviour with distance to the shower axis, shower zenith angle and azimuthal position with respect to the incoming shower direction. Also the different contributions to the electromagnetic particle densities differ from each other as will be shown below.

Firstly, we have studied the EM and muon number densities as a function of the distance to the shower axis (lateral distributions) in 10 EeV proton-induced showers at different zenith angles, averaging over the azimuthal angle ζ on the ground. We have also parameterised the lateral distributions of the particle densities as a function of shower zenith angle for practical applications, using 10 EeV proton showers simulated with the hadronic model QGSJET01 as reference. These parameterisations are presented in Appendix A. The results from these parameterisations are shown as solid lines in the top panels of Fig. 6 compared to the simulations. The simulations are reproduced by the fits without significant deviations as shown in the bottom panels of Fig. 6 ($< 10\%$ for muons and $< 30\%$ for the EM component).

3.2.1. Muonic component

As shown in the left panel of Fig. 6, the muonic density ρ_μ decreases with θ, because muons need to travel larger distances before reaching ground arriving at larger distances to the core and being spread over a larger area. This is mainly due to the transverse momentum inherited from its parent hadron. Muons of

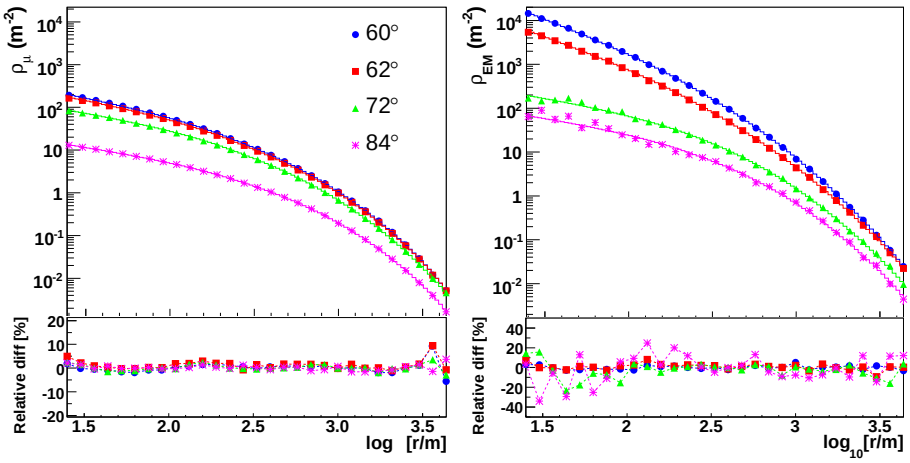

Figure 6: Top panels: Muonic (left panel) and electromagnetic (right panel) particle densities as a function of the distance to the shower axis in the shower plane for 10 EeV proton showers at different zenith angles simulated with the QGSJET01 hadronic model. For a fixed r the densities were averaged over the azimuth angle ζ. The solid lines indicate the results of the fitting functions in Appendix A. Bottom panels: Relative difference in % between the muonic (left panel) and electromagnetic (right panel) densities as obtained with the parameterisations in Appendix A with respect to the simulations.

the lowest energies typically decay, decreasing further the density with theta, especially at large distances.

Both effects also explain the behaviour of the muon energy distribution with θ and distance to the shower axis shown in Fig. 1. For example, in the right panel of this figure one can see that the mean muon energy increases with θ for a fixed r, because only the more energetic muons survive and besides, these deviate more from the shower axis.

3.2.2. Electromagnetic component

The behaviour of the electromagnetic lateral distribution in inclined showers (right panel of Fig. 6), can be qualitatively understood as a combination of the different behaviour of the two contributions to the EM component namely, that produced by π^0 decay (from hadronic origin) and the electromagnetic halo (from muonic origin).

Separating the two main contributions to the total EM density is not possible in AIRES simulations because the information on the mother particle (a π^0 or a muon) producing the EM subshower is lost. However we have devised a procedure to obtain in an approximate way the various contributions to the total EM density. The total EM density $\rho_{\rm EM}$ can be obtained as:

$$\rho_{\rm EM} = \rho_{\rm EM}^{\rm em\ shower} + \rho_{\rm EM}^{\mu\ \rm decay} + \rho_{\rm EM}^{\mu\ \rm int} \qquad (1)$$

where $\rho_{\rm EM}^{\rm em\ shower}$ is the EM density due to decay of π^0s produced in hadron and meson interactions, $\rho_{\rm EM}^{\mu\ \rm decay}$ is the EM density due to muon decay and

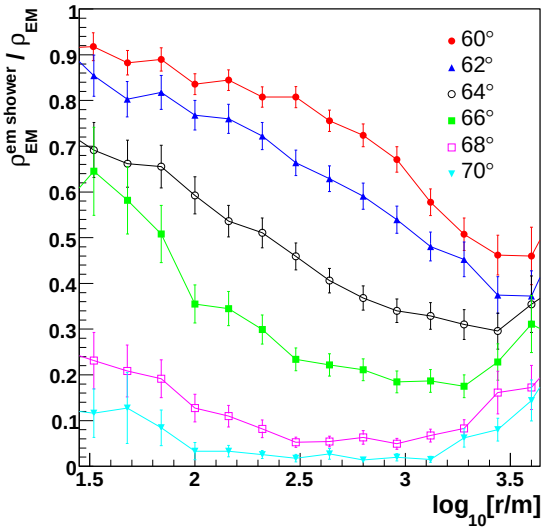

Figure 7: Contribution of the electromagnetic particle density due to π^0 decay of hadronic origin in the shower (remnant EM shower) to the total EM density as a function of distance to shower axis for different zenith angles. This component was obtained in special simulations in which muons are not explicitly followed so that they cannot contribute to the EM halo (see text for details).

$\rho_{\rm EM}^{\mu\ {\rm int}}$ is the EM density due to muon bremsstrahlung, pair production and nuclear interactions. Using AIRES we have performed a special subset of shower simulations in which we artificially set the muon energy threshold above which muons are explicitly followed in the simulations to a very high energy (10 TeV), and at the same time we set the muon lifetime to infinity so that muons never decay. The last condition needs to be forced otherwise muons are artificially decayed in AIRES. The EM density obtained in this way has no contribution from muons (i.e. $\rho_{\rm EM}^{\mu\ {\rm decay}} + \rho_{\rm EM}^{\mu\ {\rm int}} \simeq 0$) and can only be generated in π^0 decays (produced in hadron and meson interactions). In Fig. 7 we show the lateral distribution of the EM density as obtained in these simulations for different zenith angles. It can be seen that as the zenith angle increases from 60° the EM density due to π^0 decay is increasingly absorbed, until the zenith angle reaches $\sim 70°$ and it practically disappears, except for a small contribution still reaching ground very near the core at $r < 100$ m and far from it at $r > 2$ km reaching only the early region of the shower.

For $\theta > 70°$ the EM component from π^0 decay is negligible and the EM halo dominates at essentially all distances to the core. This is reflected in the fact that the EM lateral distribution follows the behaviour of the muonic one. This is more apparent in Fig. 8 where the ratio of the electromagnetic and muonic densities is shown. Note that the results shown in this figure are obtained with standard AIRES simulations.

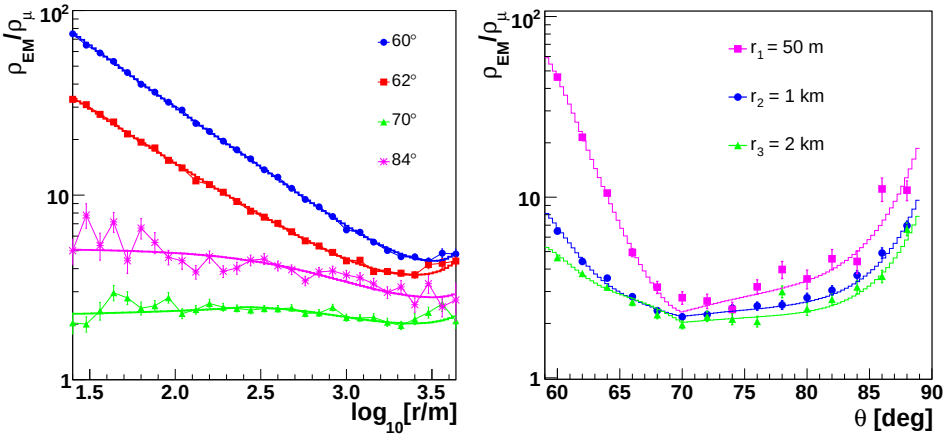

Figure 8: Left panel: The ratio of the electromagnetic to muonic particle densities as a function of the distance from the shower axis in the shower plane for different zenith angles. Right panel: The ratio of the electromagnetic to muonic particle densities as a function of the shower zenith angle for different distances from the shower axis. The simulations were performed for 10 EeV proton showers in absence of geomagnetic field. The solid line indicates the ratio of the results given by the fitting functions in Appendix A.

4. The ratio of the electromagnetic to muonic contributions to the densities

We have also studied the behaviour of the ratio of the electromagnetic to the muonic densities:

$$R_{\mathrm{EM}/\mu} = \rho_{\mathrm{EM}}/\rho_\mu \tag{2}$$

In Fig. 8, we show $R_{\mathrm{EM}/\mu}$ averaged over azimuth angle ζ as a function of the distance to the core r for different shower zenith angles θ and as a function of the θ for different fixed distances as obtained in the simulations, and the ratio predicted by the parameterisations proposed in Appendix A. Near the core, the ratio decreases with zenith angle from $\theta = 60^\circ$ to $\sim 70^\circ$ due to the increasing absorption of the EM component from π^0 decay, and then increases again with θ as can be seen in Fig. 8, mainly due to muon hard interactions processes that are expected to dominate near the core in very inclined showers. Far from the core the lateral distribution of the ratio tends to flatten due to the dominant contribution of the EM halo produced by muon decay in flight. The larger the zenith angle, the closer to shower core the ratio levels off. The slight increase of the ratio for $\theta \lesssim 68^\circ$ and far from the core ($r \gtrsim 2$ km) is attributed to the combination of two effects, one is that the number of low energy muons decreases more rapidly at large distances because they decay before reaching the ground, and only energetic muons survive, and on the other hand the presence of the contribution to the EM density due to π^0 decay, particularly in the early region of the shower.

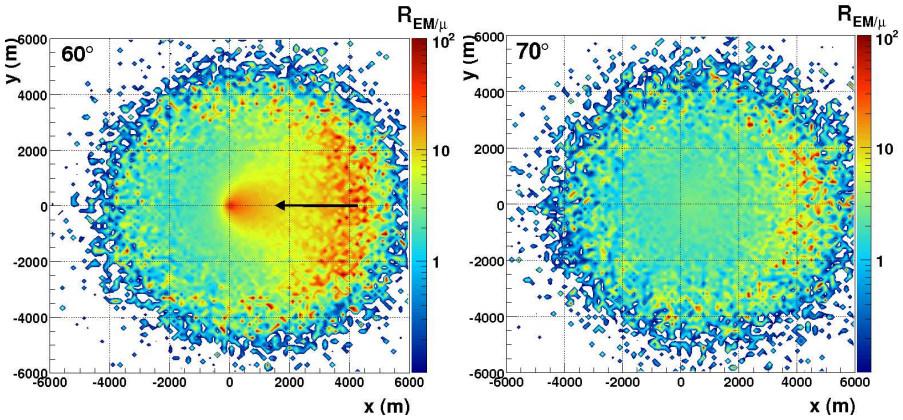

Figure 9: Map of the ratio $R_{\mathrm{EM}/\mu}$ in the shower plane for 10 EeV proton showers at $\theta = 60°$ (left panel) and $\theta = 70°$ (right panel). The arrow indicates the shower direction projected on the ground. The shower core hits ground at the position (x=0,y=0).

4.1. Azimuthal asymmetry in the ratio of the electromagnetic to muonic densities

In addition to the dependence on zenith angle and distance to shower core, we have also studied the azimuthal asymmetry of $R_{\mathrm{EM}/\mu}$. For the moment the effect of the geomagnetic field is neglected.

In the left panel of Fig. 9, we show the 2-dimensional map of the ratio $R_{\mathrm{EM}/\mu}$ in the shower plane for 10 EeV proton showers at $\theta = 60°$. The shower incoming direction is from East to West in the figure. As expected, there is a clear azimuthal asymmetry at a fixed distance to the core. The contribution of the electromagnetic component is larger in the early region. However, as shown in the right panel of Fig. 9, at zenith angles $\theta \geq 70°$ the azimuthal asymmetry is less significant because only muons accompanied by the electromagnetic halo arrive at ground. Since these two components approximately have the same asymmetry (section 3.1.2), the final asymmetry is practically canceled out when making their ratio.

To study further the azimuthal dependence of the asymmetry we divide the shower plane in bins of width $\Delta\zeta = 30°$ centered around ζ, and we calculate the lateral distributions of the ratio in each bin for a fixed zenith angle: $R_{\mathrm{EM}/\mu}(r, \theta, \zeta)$, and we compare these distributions to the distribution $\langle R_{\mathrm{EM}/\mu}\rangle(r, \theta)$ obtained averaging over ζ. For this purpose we define the asymmetry parameter Δ_ζ as

$$R_{\mathrm{EM}/\mu}(r, \theta, \zeta) = \langle R_{\mathrm{EM}/\mu}\rangle(r, \theta) \times (1 + \Delta_\zeta) \tag{3}$$

In Fig. 10, we show the lateral distribution of $R_{\mathrm{EM}/\mu}$ in different ζ bins compared to the mean value (left panel) and their corresponding asymmetry

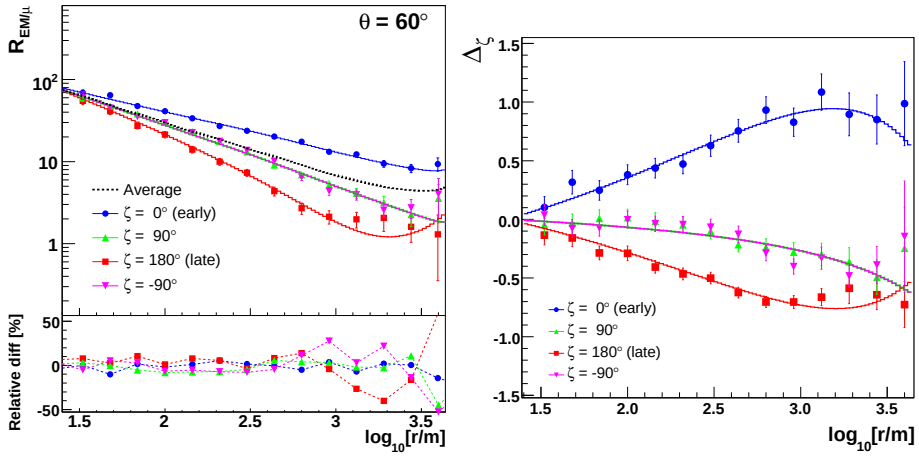

Figure 10: Left panel: The ratio $R_{\mathrm{EM}/\mu}$ as a function of the distance from the shower axis in the shower plane in different bins in ζ for 10 EeV proton showers with $\theta = 60°$. The relative difference in % between the ratio as obtained with the parameterisation in Appendix B with respect to the simulations is shown in the bottom panel. Right panel: Asymmetry of the lateral distribution of the ratio $R_{\mathrm{EM}/\mu}$ in different ζ bins. The size of the bins is $\Delta\zeta = 30°$ centered at ζ. The solid line indicates the ratio of the results given by the fitting functions in Appendix B.

parameter Δ_ζ (right panel) for showers at $\theta = 60°$. $|\Delta_\zeta|$ increases with distance to the core and it is larger in the early region than in the late region as expected.

In addition to the dependence on position in the shower plane (r, ζ), the asymmetry parameter Δ_ζ also depends on the shower zenith angle. In Fig. 11 we show Δ_ζ as a function of ζ for a fixed distance $r = 1000$ m and different zenith angles. The amplitude of the asymmetry decreases as the zenith angle increases for the reasons explained above. This plot illustrates the importance of accounting for the asymmetry in the ratio when dealing with inclined showers with $60° < \theta < 70°$.

We have parameterised the asymmetry Δ_ζ as a function of the distance to the core, zenith angle and the azimuthal angle ζ accounting for all the dependences above (see Appendix B). As an example, we show the results of the fit as solid lines in Fig. 10. The simulations are reproduced by the fit without significant deviations as shown in the bottom panel of Fig. 10. In the parameterisation, we have assumed that the azimuthal asymmetry $\Delta_\zeta \simeq 0$ is negligible when $\theta > 68°$.

4.2. Geomagnetic field effect on the ratio of the electromagnetic to muonic densities

As discussed before (section 3.1.1), the muon distributions are distorted by the presence of the geomagnetic field for zenith angles greater than $\theta \sim 75°$.

At these angles, the dominant contribution to the electromagnetic component at ground is due to the electromagnetic halo, which inherits the muon

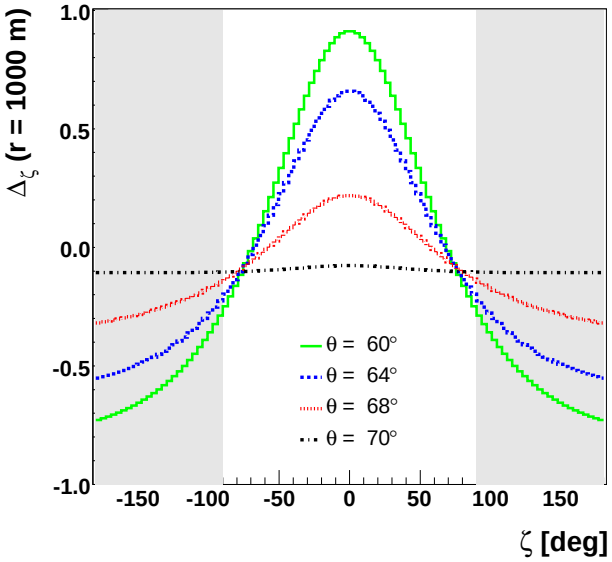

Figure 11: Asymmetry of the ratio $R_{\mathrm{EM}/\mu}$ as a function of the azimuth angle in the shower plane ζ at $r = 1000$ m and for different θ. The shaded area indicates the late region of the shower and the remaining area corresponds to the early region.

spatial distribution and is proportional to the muonic density, and we expect the ratio of the electromagnetic to muonic densities to maintain the symmetry in the azimuthal angle ζ. For this reason, we have only studied the effect of the geomagnetic field on the ratio averaging over the azimuthal angle ζ in the shower plane, for different shower zenith θ and azimuth ϕ angles. More precisely, for each θ we study the extreme cases where the effect is minimal, $\phi \approx 90^\circ$, and maximal, $\phi \approx 0^\circ$ (or 180°), where ϕ is defined as in Fig. 2. In the left panels of Fig. 12 we show the lateral behaviour of $R_{\mathrm{EM}/\mu}$ in the presence of the geomagnetic field for 10 EeV proton showers. We also plot the relative difference between $R_{\mathrm{EM}/\mu}$ with and without geomagnetic field effect, namely:

$$\Delta R_B = \frac{R_{\mathrm{EM}/\mu}(\phi) - \langle R_{\mathrm{EM}/\mu}\rangle(B=0)}{\langle R_{\mathrm{EM}/\mu}\rangle(B=0)} \tag{4}$$

As can be seen in the right panels of Fig. 12, the effect of the geomagnetic field on $R_{\mathrm{EM}/\mu}$ is more important near the core at all zenith angles. The reason for this is that only the highest energy muons are not significantly deflected and stay close to the core, and these are more likely to suffer hard interactions and induce an electromagnetic shower. As a consequence ρ_{EM} increases and at the same time ρ_μ decreases because lower energy muons are being deflected away from the core. These two effects produce an overall increase in $R_{\mathrm{EM}/\mu}$. This increase is small for $\theta \leq 78^\circ$ and $r > 100$ m, with $\Delta R_B \lesssim 20\%$. When $\theta = 80^\circ$ the effect starts to be important in the case of maximal deviation ($\phi = 180^\circ$)

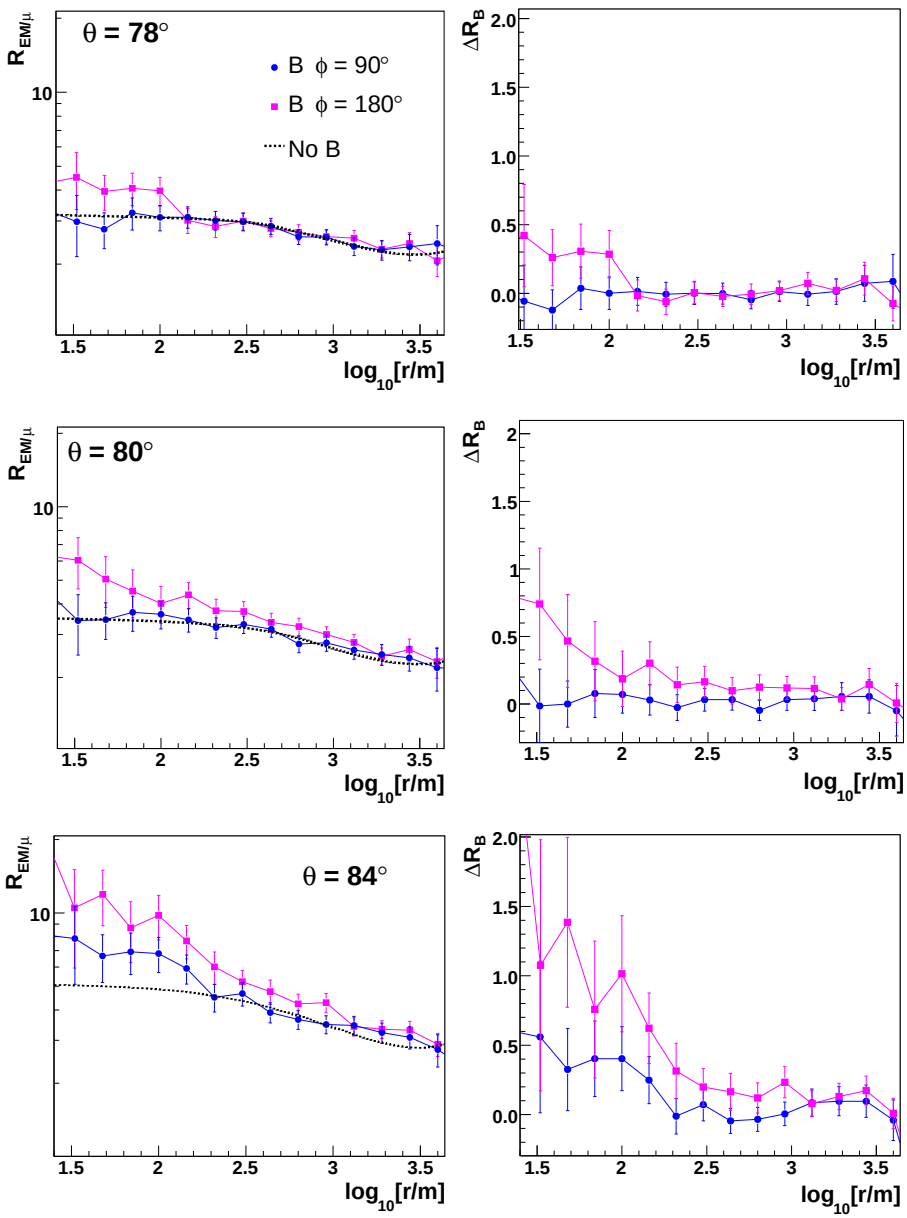

Figure 12: Left panel: The ratio $R_{\mathrm{EM}/\mu}$ as a function of the distance from the shower axis in the shower plane for 10 EeV proton showers for different θ and $\phi = 90°$ (circles) and $\phi = 180°$ (squares) in the presence of the geomagnetic field. The lateral behaviour of the ratio without the effect of the geomagnetic field is also shown (dashed line). Right panel: The relative difference with respect to the ratio as obtained without the geomagnetic field (see text).

where $\Delta R_B > 20\%$ for $r < 200$ m, whereas for the case of minimal expected deviation ($\phi = 90°$) the relative difference remains smaller at all distances. At larger angles $\theta > 80°$, the geomagnetic field has a strong influence on $R_{\mathrm{EM}/\mu}$, even when $\phi \approx 90°$ and the effect is expected to be minimal. It can also be seen that the larger the zenith angle, the farther from the shower core the influence of the geomagnetic field is still important for the reasons explained before.

In conclusion, the effect of the geomagnetic field on the ratio of the electromagnetic to muonic number densities can be considered relevant for showers at $\theta \gtrsim 84°$. It should be noted that the rate of events at such high zenith angles detected at ground level by an array of detectors is small due to the reduced solid angle and the small size of the projection of the array onto the direction of the shower, so that this effect can be ignored for the purposes of data analysis in a first approximation.

5. Dependence of the ratio on primary energy, mass composition and hadronic model

In this section we study the dependence of $R_{\mathrm{EM}/\mu}$ on primary energy, mass of the primary cosmic ray initiating the shower, and hadronic interaction model used to perform the simulations. These dependences are studied neglecting the effect of the geomagnetic field and averaging over azimuthal angle ζ in the shower plane.

5.1. Energy dependence

The more energetic a shower, its maximum occurs deeper in the atmosphere, and therefore, the shower components are in a younger stage of evolution. The lateral distribution of the electromagnetic and muonic densities exhibits a characteristic behaviour with energy and depth of shower maximum [23]. The lateral distribution of the charged electromagnetic component due to the cascading processes (mainly due to π^0 decay) is approximately given by,

$$\rho_e = N_e(E_0, X - X_{max})\ f_e(r, X - X_{max}) \tag{5}$$

where the total number of particles N_e depends on primary energy E_0 as $N_e \propto E_0^{\alpha}$. At shower maximum, $\alpha \simeq 1$ [24]. The lateral behaviour of the electromagnetic component f_e depends on shower age $(X - X_{max})$.

On the other hand, the lateral distribution of muons can be expressed as:

$$\rho_\mu = N_\mu(E_0, X - X_{max})\ f_\mu(r) \tag{6}$$

where the total number of muons $N_\mu \propto E_0^{\beta}$ (with $\beta < 1$) increases slower with the energy than the electromagnetic component [25]. Also the lateral behaviour f_μ is approximately independent of the shower age [23].

Finally, as discussed before, the electromagnetic component due to muon decay in flight is proportional to the muonic density. Hence, the lateral distribution of this component is expected to have the same energy dependence as the muonic one.

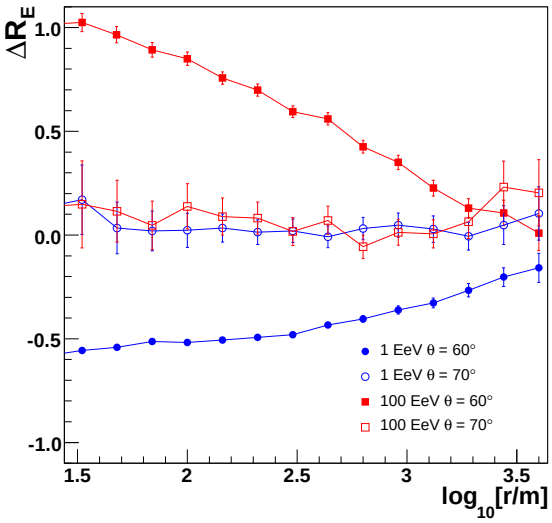

Figure 13: The relative difference ΔR_E between the ratio $R_{\mathrm{EM}/\mu}$ obtained in 1 EeV and 100 EeV proton-induced showers with respect to that obtained in 10 EeV proton shower simulations. ΔR_E is shown as a function of distance to shower core r at zenith angles $\theta = 60°$ and $\theta = 70°$.

Combining all these facts, we expect the ratio $R_{\mathrm{EM}/\mu} = \rho_{\mathrm{EM}}/\rho_\mu$ to have a different behaviour depending on whether the electromagnetic component due to π^0 decay or the EM halo contributes more to the total electromagnetic density. We study the energy dependence of $R_{\mathrm{EM}/\mu}$ performing the relative difference between the ratio at a given energy with respect to that obtained for 10 EeV proton showers, $\langle R_{\mathrm{EM}/\mu}\rangle$ (see previous section):

$$\Delta R_E = \frac{R_{\mathrm{EM}/\mu}(E) - \langle R_{\mathrm{EM}/\mu}\rangle(10\ \mathrm{EeV})}{\langle R_{\mathrm{EM}/\mu}\rangle(10\ \mathrm{EeV})} \tag{7}$$

In Fig. 13 we show ΔR_E for $E = 1$ EeV and 100 EeV showers. At $\theta = 70°$, the energy dependence of the ratio is small $\Delta R_E \lesssim 20\%$, because the electromagnetic density being dominated by the contribution from the EM halo, is roughly proportional to the muonic density, regardless of the shower energy. However for $\theta = 60°$ there is a dependence of ΔR_E on the shower energy, especially close to the shower core where the EM component due to cascading processes contributes more to the EM density (see also Fig. 7). In this angular range, we expect $R_{\mathrm{EM}/\mu}$ to behave as $\propto E_0^{\alpha/\beta}$ and hence to depend on shower energy. As can be seen in Fig. 13, ΔR_E is larger (smaller) for 100 EeV (1 EeV) showers than at 10 EeV because of the larger (smaller) EM component coming from the cascading processes in the shower which penetrates more (less) in the atmosphere.

The dependence of ΔR_E on θ is studied in more detail in Fig. 14, where we plot ΔR_E in different bins of r, as a function of θ for 1 EeV and 100 EeV proton showers. Here, we confirm what was said before, for zenith angles above $\sim 70°$

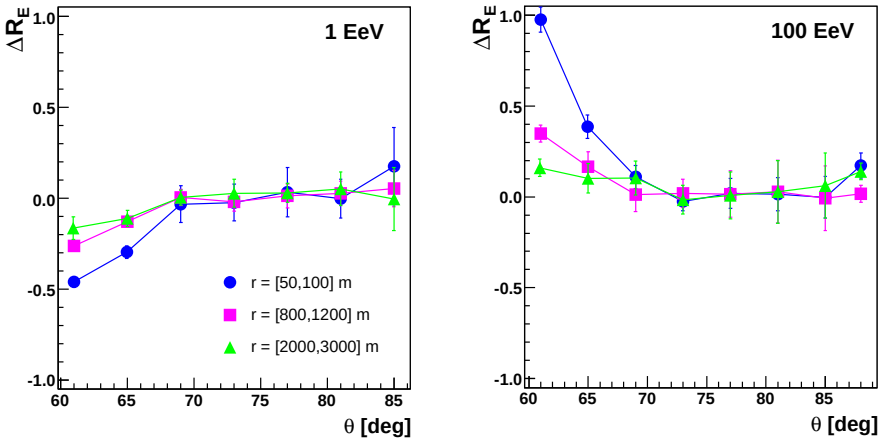

Figure 14: The relative difference ΔR_E between the ratio $R_{\mathrm{EM}/\mu}$ obtained in 1 EeV (left panel) and 100 EeV (right panel) proton-induced showers with respect to that obtained in 10 EeV proton shower simulations. ΔR_E is plotted as a function of the shower zenith angle in different bins in distance to the core r.

the EM component is only due to the EM halo and the ratio $R_{\mathrm{EM}/\mu}$ remains constant at the same level with energy, while if $\theta \lesssim 70^\circ$ there is a dependence on energy that increases as the distance to the core decreases.

5.2. Primary mass dependence

At present, the chemical composition of the cosmic rays at the highest energies (> 1 EeV) remains uncertain. Some authors claim that cosmic rays at these energies are mainly protons [26], and others discuss the possibility of heavier elements such as iron nuclei [27]. The most recent results from extensive air shower experiments do not allow to rise any firm conclusion [28, 29]. For this reason we have studied the dependence of the ratio $\rho_{\mathrm{EM}}/\rho_\mu$ on the mass of the primary particle initiating the shower accounting for protons and iron nuclei in our simulations.

Compared to a proton, an iron nucleus typically interacts higher in the atmosphere, producing a shower with a smaller depth of maximum. Also applying a simple superposition model an iron nuclei produces a shower with $\sim 30\% - 40\%$ more muons than a proton. As a result, an iron-initiated shower is expected to have a smaller electromagnetic density from cascading processes and a larger muonic density than a proton shower, and therefore a smaller $R_{\mathrm{EM}/\mu}$ as long as the EM component due to cascading processes contributes more than that due to the EM halo ($\theta < 70^\circ$ and close to the shower core). To demonstrate this, we have calculated the relative difference between $R_{\mathrm{EM}/\mu}$ in iron showers at 10 EeV with respect to that obtained in 10 EeV proton shower simulations

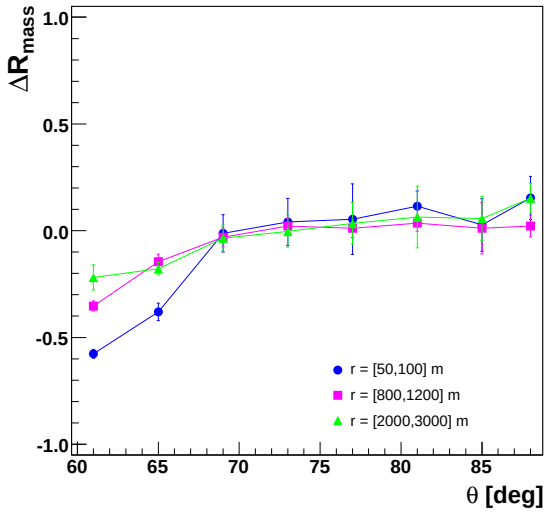

Figure 15: The relative difference $\Delta R_{\rm mass}$ between the ratio $R_{\rm EM/\mu}$ obtained in 10 EeV iron-induced shower simulations with respect to that obtained in 10 EeV proton shower simulations. $\Delta R_{\rm mass}$ is plotted as a function of the shower zenith angle in different bins in distance to the core r.

$$\Delta R_{\rm mass} = \frac{R_{\rm EM/\mu}({\rm Fe}) - \langle {\rm R_{EM/\mu}} \rangle ({\rm p})}{\langle R_{\rm EM/\mu} \rangle ({\rm p})} \tag{8}$$

In Fig. 15 we show ΔR_{mass} as a function of zenith angle in different bins of r. For reasons very similar to those that explain the energy dependence of $R_{\rm EM/\mu}$ studied before, we can explain the mass dependence. For angles larger than $\sim 70^\circ$ the dependence on the mass is negligible, because only the EM halo is present and it is proportional to the muonic density. Although the latter increases due to the larger mass of the primary, the former increases accordingly and the ratio stays roughly constant at the same level with mass. However when $\theta \lesssim 70^\circ$ we can see a clear dependence on mass, with iron showers having smaller values of $R_{\rm EM/\mu}$ due to the fact that the EM component is dominated by cascading processes and the iron-induced shower penetrates less in the atmosphere.

5.3. Hadronic model dependence

At the highest energies, there is a lack of empirical knowledge about the hadronic interactions which greatly influence shower development [30]. Laboratory experiments have studied particle collisions only at centre-of-mass energies equivalent to fixed target energies of 10^{15} eV, so assumptions must still be made to perform the interactions needed in the shower simulations at the energies of interest ($> 10^{18}$ eV). This fact leads to discrepancies between the different hadronic models on predictions of inelastic cross-sections and inelasticity (multiplicity and energy of the secondaries) (see for instance [31] for more details).

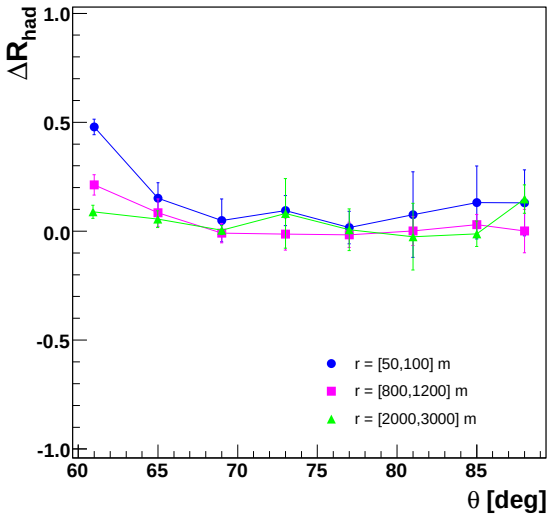

Figure 16: The relative difference $\Delta R_{\rm had}$ between the ratio $R_{\rm EM/\mu}$ obtained in 10 EeV proton-induced showers simulated with Sibyll 2.1, with respect to that obtained in 10 EeV proton showers simulated with QGSJET01. $\Delta R_{\rm had}$ is shown as a function of the shower zenith angle in different bins of distance to the shower core r.

These quantities determine to a large extent the longitudinal development of the air shower and, as a consequence, the number densities of the EM and muonic components at ground.

In this work, we compare two high energy interaction models currently used in cosmic ray physics: QGSJET01 [13] and Sibyll 2.1 [14]. For proton primaries at 10 EeV, the QGSJET model predicts showers that on average develop higher in the atmosphere and have 40% more muons than showers simulated with Sibyll. As a result, QGSJET predicts more muons at ground and a smaller electromagnetic component due to cascading processes.

Following a similar line of reasoning as in the case of the energy and mass dependence of the ratio of the EM to muonic densities, $R_{\rm EM/\mu}$ is expected to be larger for showers simulated with Sibyll at zenith angles $\lesssim 70^\circ$, and roughly independent on the model for θ larger than $\sim 70^\circ$. This behaviour can be seen in Fig. 16, where we plot the relative difference $\Delta R_{\rm had}$ between $R_{\rm EM/\mu}$ for 10 EeV proton showers simulated with Sibyll 2.1 with respect to the one obtained in showers simulated with QGSJET01:

$$\Delta R_{\rm had} = \frac{R_{\rm EM/\mu}({\rm Sibyll}) - \langle {\rm R_{EM/\mu}}\rangle({\rm QGSJET})}{\langle R_{\rm EM/\mu}\rangle({\rm QGSJET})} \qquad (9)$$

$\Delta R_{\rm had}$ is shown as a function of zenith angle in different bins of r, to make the increasingly larger differences between Sibyll and QGSJET for small distances to the shower axis more apparent, as expected from the dominance of the EM component due to cascading processes near the core.

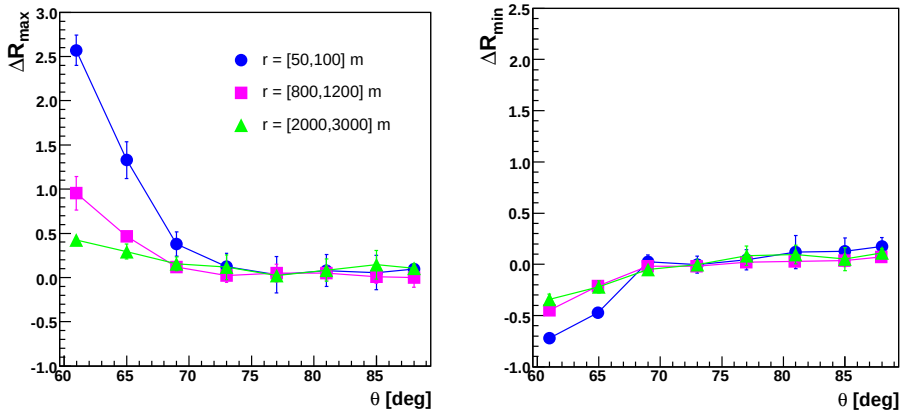

Figure 17: The maximum $\Delta R_{\rm max}$ (left panel) and minimum $\Delta R_{\rm min}$ (right panel) relative differences in the ratio $R_{\rm EM/\mu}$ obtained respectively for 100 EeV proton showers simulated with Sibyll 2.1 and 1 EeV iron showers simulated with QGSJET01, with respect to proton showers at 10 EeV energy simulated with QGSJET01. $\Delta R_{\rm max}$ and $\Delta R_{\rm min}$ are both shown as a function of the shower zenith angle in different bins in distance to the shower core r.

5.4. Summary and discussion

Summarizing this section, we have studied the effect of energy, mass composition and hadronic interaction model on the ratio of electromagnetic to muonic densities in absence of geomagnetic field effect, using the ratio obtained for 10 EeV proton showers simulated with QGSJET01 as reference. Combining all these dependences, we find that the extreme differences with respect to the reference ratio correspond to:

- Maximum: 100 EeV proton showers simulated with Sibyll 2.1.
- Minimum: 1 EeV iron showers simulated with QGSJET01.

In Fig. 17 we show the relative differences between both cases and the reference ratio ($\Delta R_{\rm max}$ and $\Delta R_{\rm min}$) as a function of θ in different bins in r. The figure illustrates the extreme cases in the dependency of $R_{\rm EM/\mu}$ on energy, mass and model one should expect.

6. Fluctuations of the particle densities

In this section, we attempt to estimate the effect of physical fluctuations on the muon and electromagnetic number densities using simulations. The particle densities in individual showers are affected by different sources of fluctuation, namely:

- Physical (intrinsic) "shower-to-shower" fluctuations due to fluctuations in the atmospheric depth of the first interactions in the shower, fluctuations in secondary particle production, etc., in general fluctuations in the cascading processes during the development of the shower.

- "Artificial" fluctuations due to the thinning procedure in the shower simulation.

The ideal way of computing the "shower-to-shower" fluctuations of the electromagnetic and muonic components is to perform full (non-thinned) shower simulations. This is unfortunately not feasible due to the large computing time and huge disk space needed to store the information on particles at ground at the highest energies (even for a single shower). One has to rely on thinned simulations in which artificial fluctuations are introduced. To overcome this problem, we have devised a simple approach based on a method given in [32] to estimate how physical fluctuations affect the electromagnetic and muonic particle distributions when obtained from tracked particles with weights w_i. Here, we neglect the azimuthal asymmetry of the densities and obtain the densities in concentric rings in r around the shower core of area $A_{\rm r}$.

The particle density corresponding to n particles with individual weights w_i falling in an area $A_{\rm r}$ is calculated as:

$$\rho = \sum_{i=1}^{n} \frac{w_i}{A_{\rm r}} = \frac{N}{A_{\rm r}} \tag{10}$$

so that the fluctuations of the particle densities stem from the fluctuations in the total particle number after accounting for the weights: $\sigma_\rho \approx \sigma_N$. Defining the average weight of the n particles falling in a ring of area $A_{\rm r}$ as $\overline{w} = \sum_{i=1}^{n} w_i/n$, the unweighted particle number can be approximated as $N \simeq \overline{w}n$ and the standard deviation of N can be expressed as:

$$\sigma_N^2 = \langle N^2 \rangle - \langle N \rangle^2 = \langle \overline{w}^2 n^2 \rangle - \langle \overline{w} n \rangle^2 \tag{11}$$

Assuming that the mean particle weight does not fluctuate from shower to shower as in the ideal case of an unthinned shower, and taking it to be equal to the average weight over all the particles followed explicitly in the shower simulation, we obtain:

$$\sigma_N^2 = \overline{w}^2 \left(\langle n^2 \rangle - \langle n \rangle^2 \right) = \overline{w}^2 \sigma_n^2 \tag{12}$$

Eq. 12 represents an approximate way of obtaining the intrinsic physical shower-to-shower fluctuations of the muonic and electromagnetic particle densities from Monte Carlo simulations, which gives a good account of the physical fluctuations for thinning levels smaller than $\sim 10^{-6}$ [33]. In fact, in the case of an unthinned shower, in which only the intrinsic fluctuations should be present, $\bar{w} = 1$, $N = n$ and Eq. 8 gives $\sigma_N^2 = \sigma_n^2$ as expected.

In Fig. 18 we show the relative physical fluctuations ($\sigma^{\rm rel} = \sigma_\rho/\rho$) of the electromagnetic (top) and muon (bottom) densities as a function of the distance to the shower core for 10 EeV proton showers at different zenith angles. These have been computed obtaining first σ_n^2 and $\overline{w}^2$ from the simulations and then applying Eq. 12. The fluctuations in the muonic component are roughly independent of r in the wide range of distances to the core plotted in the figure,

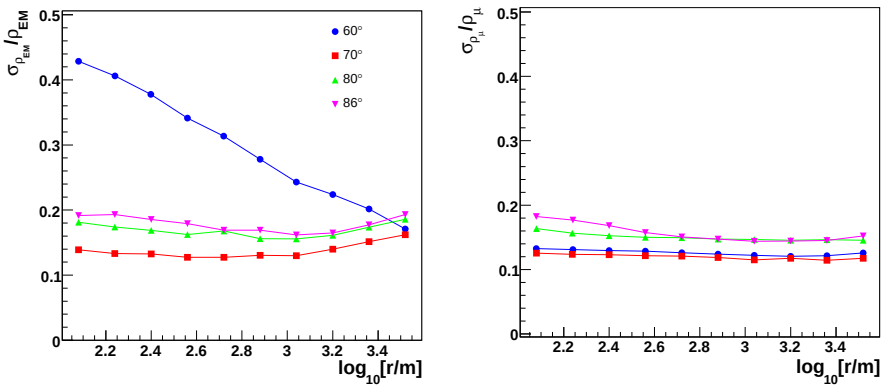

Figure 18: Estimated relative physical fluctuations of the electromagnetic (left panel) and muonic (right panel) densities at ground level as a function of the distance to the shower core in the shower plane, obtained in 10 EeV proton showers simulated with AIRES + QGSJET01 and with a thinning level of 10^{-7}.

and remain at the level of $\lesssim 20\%$. On the other hand, the fluctuations in the electromagnetic component seem to depend on the contribution of the EM halo. At $\theta = 60°$ the decrease of the relative fluctuations as the distance to the core increases could be interpreted as the EM halo is becoming the dominant contribution to the EM density and mimicking the behaviour of the fluctuations in the muonic component. Similarly, for $\theta \geq 70°$ the fluctuations mimic the behaviour of those of the muonic component, they are roughly independent of r and remain at the level of $\lesssim 20\%$.

7. Summary and conclusions

We have studied the characteristics of the particle densities of the electromagnetic and muon components of inclined showers at the ground level using Monte Carlo simulations. We have shown that the electromagnetic component is composed of several sub-components originated in cascading and muonic processes. These different contributions to the electromagnetic component differ from each other on their behaviour with distance to the core, zenith angle and angular position (ζ).

We have studied the ratio of the electromagnetic to muon densities ($R_{\mathrm{EM}/\mu}$) as a function of several parameters. Firstly, we have characterised the dependence of this ratio on the distance to the core and shower zenith angle (see Fig. 8). Near the core up to $\theta \sim 70°$ its behaviour is explained by the increasing absorption of the contribution to the EM component due to π^0 decay and beyond 70° by the dominance of the contribution to the EM component due hard muon processes. Far from the core (> 1 km), the ratio is compatible with an almost constant value because the electromagnetic component due to muon decay in flight dominates the electromagnetic density at ground. Then, we have

studied the dependence of $R_{\mathrm{EM}/\mu}$ on the azimuthal position ζ. For showers with $60^\circ < \theta < 70^\circ$ we have found an azimuthal asymmetry, which is mostly due to the longitudinal development effect. Moreover, we have studied the effect of the Earth magnetic field in this ratio finding that is important for showers at $\theta \gtrsim 84^\circ$.

Considering all these dependences above and neglecting the geomagnetic field effect, we propose a parameterisation of the $R_{\mathrm{EM}/\mu}(r, \theta, \zeta)$ that predicts the simulated data to a good precision level (see Fig. 10). The fits are valid for 10 EeV proton showers simulated with the hadronic model QGSJET01, and in the ranges $\theta \in [60^\circ, 89^\circ]$ and $r \in [20, 4000]$ m.

We have characterised the dependence of this ratio with the primary energy, the primary mass composition and the hadronic interaction model used in the simulations. The general result is that at zenith angles $\gtrsim 70^\circ$ the ratio remains constant because only the electromagnetic halo contributes to the electromagnetic component.

Finally, we have estimated the effect of physical fluctuations on the electromagnetic and muon densities. The muon fluctuations remain roughly constant at the level of $\lesssim 20\%$. While, the EM fluctuations depend on the dominance of the electromagnetic halo on the EM component, and tend to be constant $\lesssim 20\%$ for higher zenith angles.

In Table 1 we summarise some results for two different distances to the core and different shower zenith angles. Note that in the angular region $60^\circ < \theta < 70^\circ$ the presence of the remnant of the electromagnetic shower due to cascading processes from π^0 decay of hadronic origin entails important dependences of the ratio on the energy, mass composition and hadronic model. Therefore, this region could be the most suitable one for studies about composition and hadronic interaction models by means of the electromagnetic component in the shower at ground level. However in the region $\theta \gtrsim 70^\circ$ the ratio is not sensitive to composition and hadronic model, and this angular region might be in principle more suitable to study the UHECR energy spectrum with inclined events detected by ground detectors.

8. Acknowledgments

The authors thank Gonzalo Rodríguez-Fernández and our colleagues of the Pierre Auger Collaboration for support and discussions on this topic. The Helmholtz association, Germany (HHNG-128 grant), Ministerio de Ciencia e Innovación (FPA 2007-65114), the Spanish Consolider-Ingenio 2010 Programme CPAN (CSD2007-00042), Xunta de Galicia (PGIDIT 06 PXIB 206184 PR) and Consellería de Educación (Grupos de Referencia Competitivos – Consolider Xunta de Galicia 2006/51), and FEDER Funds, Spain, are acknowledged for providing funding. Inés Valiño gratefully acknowledges the financial support from "Fundación Pedro Barrié de la Maza" (Spain). The authors also thank CESGA (Centro de Supercomputación de Galicia) for computing resources.

r (m)	θ (deg)	$\Delta R_{B_{\phi=180^\circ}}$	$\Delta R_{E=100EeV}$	$\Delta R_{\rm mass}$	$\Delta R_{\rm had}$	$\sigma^{\rm rel}_{\rho_{\rm EM}}$	$\sigma^{\rm rel}_{\rho_\mu}$
100	60	-2	83	-61	40	45	13
	70	7	6	5	11	14	12
	80	29	-2	5	1	17	16
1000	60	-2	33	-42	19	26	13
	70	7	4	2	3	14	12
	80	9	-2	-2	-1	17	15

Table 1: Summary of the dependences of the ratio of EM to muonic component on the geomagnetic field, energy, primary mass and hadronic model, using protons at $E = 10^{19}$ eV simulated with the QGSJET01 model and with no geomagnetic field as reference (see Eqs. 4, 7, 8 and 9 for the definitions of the different ΔR). The dependences are given at different distances from the shower axis 100 m and 1 km, and different zenith angles 60°, 70° and 80°. We also give the relative physical fluctuations of the EM and muonic components as obtained with Eq. 12. The results are given in percentage %.

A. Parameterisation of the muonic and electromagnetic particle densities

We give here the parameterisations performed for the lateral distributions of the electromagnetic and muonic densities at ground level projected onto the shower plane. The densities are given as a function of distance to the core r in the shower plane and shower zenith angle θ, averaging over the azimuthal angle ζ. In Appendix B we also give a parameterisation of the azimuthal asymmetry.

The fits are valid for 10 EeV proton showers simulated with the hadronic model QGSJET01, and in the ranges $\theta \in [60^\circ, 89^\circ]$ and $r \in [20, 4000]$ m.

A.1. Muonic component

We have used two different functional forms to account for the different behaviour of the lateral distributions at large distances from the core. Near the core, we use a form based on the Vernov functional form [34] and for larger distances a function based on the Nishimura-Kamata-Greisen functional form [35, 36]:

$$\rho_\mu(r) = \begin{cases} A'\, r^{-B'} \exp(-\frac{r}{C'}) & \text{for } r < r_0 \\ A \left(\frac{r}{B}\right)^{-C} \left(1 + \frac{r}{B}\right)^{-D} + E & \text{for } r \geq r_0 \end{cases} \tag{13}$$

with $r_0 = 250$ m. All the parameters, except $B = 2000$ m and $D = 4.64$, depend on θ.

For distances $r > r_0$, the parameters can be fitted with:

$$A = 0.221 + 6.490\cos\theta\ - 14.290\cos^2\theta + 61.693\cos^3\theta - \ 66.426\cos^4\theta$$

$$C = 0.460 + 2.646\cos\theta - 5.550\cos^2\theta + 4.927\cos^3\theta$$

$$E = 10^{-4} \times \begin{cases} (-4.2 - 23.0\cos\theta + 174.8\cos^2\theta - 419.9\cos^3\theta) & \text{for } \theta < 76^\circ \\ (-4.8 - 0.3\cos\theta - 9.1\cos^2\theta) & \text{for } \theta \geq 76^\circ \end{cases}$$

For distances $r < r_0$, the parameters can be fitted with:

$$A' = \frac{\rho_\mu(r_0)}{r_0^{-B'} \exp(-r_0/C')}$$

$$B' = 0.438 + 1.978\cos\theta - 11.593\cos^2\theta + 29.724\cos^3\theta - 24.553\cos^4\theta$$

$$C' = 417.594 - 953.421\cos\theta + 1960.080\cos^2\theta - 1342.210\cos^3\theta$$

A.2. Electromagnetic component

We have fitted the lateral distribution of the electromagnetic component to the same functional forms used for the muonic component (see Eq. 13) and in the same radial ranges. In this case, the parameters show a different dependence on the zenith angle below and above $\theta = 70°$, reflecting the dominance of the contribution of the EM halo to the total EM density.

For distances $r > r_0$, $B = 1200$ m and the remaining parameters can be fitted with:

$$A(\theta) = \begin{cases} \exp(-13.120 + 33.372\cos\theta) + 30.497 - 44.807\cos\theta & \text{for } \theta < 70° \\ 8.518 - 39.824\cos\theta + 294.769\cos^2\theta - 350.548\cos^3\theta & \text{for } \theta \geq 70° \end{cases}$$

$$C(\theta) = \begin{cases} 22.228 - 167.812\cos\theta + 423.455\cos^2\theta - 340.857\cos^3\theta & \text{for } \theta < 70° \\ 0.512 + 1.051\cos\theta - 1.207\cos^2\theta & \text{for } \theta \geq 70° \end{cases}$$

$$D(\theta) = \begin{cases} -14.057 + 176.968\cos\theta - 531.461\cos^2\theta + 494.975\cos^3\theta & \text{for } \theta < 70° \\ 4.104 & \text{for } \theta \geq 70° \end{cases}$$

$$E(\theta) = \begin{cases} 0.020 - 0.084\cos\theta + 0.069\cos^2\theta & \text{for } \theta < 70° \\ -0.001 & \text{for } \theta \geq 70° \end{cases}$$

For distances $r < r_0$, $C' = 284$ m and the remaining parameters can be fitted with:

$$A'(\theta) = \frac{\rho_{EM}(r_0)}{r_0^{-B'} \exp(-r_0/C')}$$

$$B'(\theta) = \begin{cases} 0.500 + 0.580\cos\theta - 0.848\cos^2\theta & \text{for } \theta < 70° \\ 13.642 - 104.697\cos\theta + 268.581\cos^2\theta - 216.302\cos^3\theta & \text{for } \theta \geq 70° \end{cases}$$

B. Parameterisation of the azimuthal asymmetry in the ratio of the electromagnetic to muonic lateral densities

We have also parameterised the asymmetry parameter Δ_ζ. The following fits are valid for 10 EeV proton showers simulated with QGSJET01, in the ranges $\theta \in [60°, 68°]$, $\zeta \in [-180°, 180°]$ and $r \in [20, 4000]$ m. Note that the asymmetry is only important for $\theta \lesssim 70°$.

$$\Delta_\zeta = \alpha\,(r - r_0) + \beta\,(log_{10}^2 r - log_{10}^2 r_0) \tag{14}$$

where $r_0 = 20$ m.

The parameters α and β can be parameterised using a Cauchy-type function modified:

$$\alpha = -\alpha_1 \left[\frac{1}{\pi} \left(\frac{\alpha_2}{\zeta^2 + \alpha_2^2} \right) - \alpha_3 \right] \qquad \beta = \beta_1 \left[\frac{1}{\pi} \left(\frac{\beta_2}{\zeta^2 + \beta_2^2} \right) - \beta_3 \right]$$

with $\zeta \in [-180^\circ, 180^\circ]$ and:

$$\alpha_1 = -441.6080 + 20.7691\,\theta - 0.324046\,\theta^2 + 0.00167832\,\theta^3$$

$$\alpha_2 = 589.326 - 7.10\,\theta$$

$$\alpha_3 = 0.0013437$$

$$\beta_1 = -33332.80 + 1547.31\,\theta - 23.7198\,\theta^2 + 0.120283\,\theta^3$$

$$\beta_2 = 265.469 - 5.400\,\theta + 0.040\,\theta^2$$

$$\beta_3 = 10^{-5}\,(6318.27 - 196.80\,\theta + 1.58\,\theta^2)$$

References

[1] M. Ave, et al., Proc. 26$^{\text{th}}$ Int. Cosmic Ray Conference, Salt Lake City, 1 (1999), p. 365.

[2] S. Yoshida, et al., Proc. 27$^{\text{th}}$ Int. Cosmic Ray Conference, Hamburg, (2001), p. 1142.

[3] J. Abraham, et al., Nucl. Instrum. Meth. A523 (2004) 50–95.

[4] http://www.telescopearray.org.

[5] H. Kawai, et al., Nucl. Phys. Proc. Suppl. 175-176 (2008) 221–226.

[6] P. Facal San Luis [Pierre Auger Collaboration], Proc. 30$^{\text{th}}$ Int. Cosmic Ray Conference, Merida, 4 (2007), p. 339.

[7] N. Inoue [AGASA Collaboration], Proc. 26$^{\text{th}}$ Int. Cosmic Ray Conference, Salt Lake City, 1 (1999), p. 357.

[8] M. Ave, R. A. Vazquez, E. Zas, Astropart. Phys. 14 (2000) 91.

[9] D. Newton [Pierre Auger Collaboration], Proc. 30$^{\text{th}}$ Int. Cosmic Ray Conference, Merida, 4 (2007), p. 323.

[10] V. Berezinsky, A. Smirnov, Astrophys. Space Sci. 32 (1975) 461.

[11] A. N. Cillis, S. J. Sciutto, Phys. Rev. D64 (2001) 013010.

[12] S. Sciutto, http://www.fisica.unlp.edu.ar/auger/aires/.

[13] N. Kalmykov, S. S. Ostapchenko, A. I. Pavlov, Nucl. Phys. Proc. Suppl. 52B (1997) 17–28.

[14] R. Engel, et al., Proc. 26$^{\text{th}}$ Int. Cosmic Ray Conference, Salt Lake City, 1 (1999), p. 415.

[15] J. Linsley, private communication by M. Hillas (1988).

[16] A. M. Hillas, Nucl. Phys. Proc. Suppl. 52B (1997) 29–42.

[17] P. Billoir, Astropart. Phys. 30 (2008) 270–285.

[18] M. Ave, R. A. Vazquez, E. Zas, J. A. Hinton, A. A. Watson, Astropart. Phys. 14 (2000) 109–120.

[19] M. D. Ave Pernas, High Energy Air Showers, PhD Thesis, Univ. de Santiago de Compostela, Spain (1999).

[20] A. M. Hillas, et al., Proc. 11$^{\text{th}}$ Int. Cosmic Ray Conference, Budapest, 3 (1969), p. 533.

[21] Http://www.ngdc.noaa.gov/IAGA/vmod/igrf.html.

[22] M. T. Dova, L. N. Epele, A. G. Mariazzi, Astropart. Phys. 18 (2003) 351–365.

[23] T. K. Gaisser, Cosmic Rays and Particle Physics, Cambridge University Press, New York, USA, 1990.

[24] J. Matthews, Astropart. Phys. 22 (2005) 387–397.

[25] M. V. S. Rao, B. V. Sreekantan, Extensive Air Showers, World Scientific Singapore, Singapore, 1999.

[26] R. Aloisio, V. Berezinsky, P. Blasi, S. Ostapchenko, Signatures of the transition from galactic to extragalactic cosmic rays, Phys. Rev. D77 (2008) 025007.

[27] D. Allard, E. Parizot, A. V. Olinto, On the transition from Galactic to extragalactic cosmic- rays: spectral and composition features from two opposite scenarios, Astropart. Phys. 27 (2007) 61–75.

[28] T. Yamamoto [Pierre Auger Collaboration], Proc. 30$^{\text{th}}$ Int. Cosmic Ray Conference, Merida, 4 (2007), p. 335; J. Bellido [Pierre Auger Collaboration], Proc. 31$^{\text{th}}$ Int. Cosmic Ray Conference, Lodz (2009), astro-ph/0906.2319.

[29] P. Sokolsky, Nucl. Phys. Proc. Suppl. 175-176 (2008) 207–212.

[30] T. Pierog, R. Engel, D. Heck, Czech. J. Phys. 56 (2006) A161–A172.

[31] J. Knapp, D. Heck, S. J. Sciutto, M. T. Dova, M. Risse, Astropart. Phys. 19 (2003) 77–99.

[32] M. Risse, et al., Proc. 27^{th} Int. Cosmic Ray Conference, Hamburg, (2001), p. 522.

[33] P. M. Hansen, et al., Proc. 31^{th} Int. Cosmic Ray Conference, Lodz (2009), ID 0167.

[34] S. N. Vernov, et al., Can. J. Phys. 46 (1968) S197.

[35] K. Kamata, J. Nishimura, Progr. Theor. Phys. Suppl. 6 (1958) 93.

[36] K. Greisen, Ann. Rev. Nucl. Part. Sci. 10 (1960) 63–108.